Available online at www.sciencedirect.com
SCIENCE DIRECT®
International Journal of Heat and Mass Transfer 47 (2004) 3031–3045
International Journal of HEAT and MASS TRANSFER
www.elsevier.com/locate/ijhmt

Suppression of buoyancy-driven vortex flow resulting from a low speed jet impinging onto a heated disk in a vertical cylinder by cylinder top tilting

J.C. Hsieh, C.W. Cheng, T.F. Lin *

Department of Mechanical Engineering, National Chiao Tung University, Hsinchu 30010, Taiwan, ROC

Received 10 October 2003; received in revised form 28 February 2004

Abstract

Buoyancy-driven vortex flow resulting from a low speed round gas jet impinging vertically downwards onto a heated horizontal circular disk confined in an adiabatic vertical cylindrical chamber can be strong and even unstable as the buoyancy-to-inertia ratio exceeds certain critical level. An experiment combining flow visualization and temperature measurement is conducted in the present study to explore the suppression of the above buoyancy-driven vortex gas flow by inclining the top of the cylindrical chamber. The chamber top is chosen to incline linearly in the radial direction so that the mean flow in the wall-jet region is accelerated and meanwhile the effective buoyancy signified by the local Rayleigh number reduces in that direction. Specifically, in the present experiment the disk-to-chamber top separation distance decreases from 20.0 mm at the jet axis to 10.0 mm at the chamber side. Tests are conducted for the jet flow rate varied from 1.0 to 5.0 slpm (standard liter per minute) and the jet-to-disk temperature difference varied from 0 to 35.0 °C for two injection pipes with diameter 10.0 and 22.1 mm for the chambers with horizontal and inclined tops. The results from the flow visualization indicate that the chamber top inclination can effectively suppress the unstable buoyancy-induced vortex roll and the temporal flow oscillation at high buoyancy-to-inertia ratios. However, the effects of the chamber top inclination on the inertia-driven rolls are much milder. The non-monotonic air temperature distribution in the radial direction is found to result from the unique vortex flow structure in the chamber. A universal criterion based on the local flow and thermal conditions in the wall-jet region for the onset of the buoyancy-driven roll is proposed. To quantify the characteristics of the vortex flow in the chamber with the inclined top, empirical correlations have been proposed for the size and location of the vortex rolls.

1. Introduction

Complex vortex flow and thermal characteristics associated with a low speed gas jet impinging onto a heated plate are the subject of recent intensive investigation because of their relevance to the growth of semiconductor thin crystal films on silicon wafers through chemical vapor deposition (CVD) processes. In single wafer vertical CVD reactors, the chemical vapors are brought into the reactors in the form of an axisymmetric jet and then impinge onto the wafer [1]. Usually, the vapors move at relatively low speeds and the wafers are at relatively high temperatures. Under such situation strong thermal buoyancy-driven flow recirculations can be induced. Meanwhile, flow recirculation resulting from jet entrainment can appear. At sufficiently high buoyancy-to-inertia ratios the recirculating flow becomes time dependent. In an attempt to explore these complex recirculating flows, Lin and his colleagues [2,3] recently visualized the vortex flows resulting from a low speed round air jet impinging onto

* Corresponding author. Tel.: +886-03-571-2121-551; fax: +886-03-572-6-440.
E-mail address: t7217@cc.nctu.edu.tw (T.F. Lin).

0017-9310/$ - see front matter © 2004 Elsevier Ltd. All rights reserved.
doi:10.1016/j.ijheatmasstransfer.2004.02.022

Nomenclature

D_c	diameter of the processing chamber (mm)
D_j	diameter of jet at the injection pipe exit (mm)
D_w	diameter of disk (mm)
Gr	local Grashof number, $g\beta\Delta TH^3/v^2$
Gr_e	local Grashof number at the disk edge
Gr_0	Grashof number based on H_0, $g\beta\Delta TH_0^3/v^2$
g	gravitational acceleration (m/s^2)
H	vertical distance between the chamber top and heated disk in the cylinder with the inclined top (mm)
H_0	vertical distance between the exit of injection pipe and heated plate (mm)
Q_j	jet flow rate (standard liter per minute, slpm)
r_e	the radial location of the disk edge (mm)
r_s	the radial location of secondary inertia-driven roll (mm)
r, z	dimensional radial and axial coordinates (mm)
R, Z	dimensionless radial and axial coordinates, $2r/D_c$ and z/H_0
Ra	local Rayleigh number, $g\beta\Delta TH^3/\alpha v$
Ra_0	Rayleigh number based on H_0, $g\beta\Delta TH_0^3/\alpha v$
Re_j	jet Reynolds number, $\overline{V}_j D_j/v$
Re_{we}	local Reynolds number in the wall-jet region at the edge of heated disk, $\bar{u}\cdot r_e/v$
S_I	size of primary inertia-driven roll (mm)
S_O	size of buoyancy-driven roll (mm)
T_f	temperature of heated disk (°C)
T_j	jet temperature at the injection pipe exit (°C)
t	time instant (s)
t_p	period of the flow oscillation (s)
$\bar{u}$	average radial velocity of the flow at wall-jet region (m/s), $(Re_j D_j v)/(8rH)$
$\overline{V}_j$	average axial velocity of the gas jet at the injection pipe exit (m/s)

Greek symbols

α	thermal diffusivity (cm^2/s)
β	thermal expansion coefficient (K^{-1})
ΔT	temperature difference between the heated disk and the air injected into the cylinder, $(T_f - T_j)$ (°C)
v	kinematic viscosity (cm^2/s)
Φ	non-dimensional temperature, $(T - T_j)/(T_f - T_j)$

a heated horizontal circular plate confined in a vertical cylindrical chamber. They reported that the vortex flow was characterized by multiple inertia and buoyancy-driven circular rolls. At high buoyancy-to-inertia ratios the buoyancy-driven rolls become unstable and deformed to a certain degree. In the mean time new vortex rolls are generated [3]. These new rolls are highly unstable. Note that the presence of the vortex roll would result in the non-uniformities in thickness and composition for the crystal films grown from CVD processes and should be avoided in actual CVD operation. Some improvement in the reactor configuration by tapering its top wall is normally employed. The top wall inclination will accelerate the vapor flow over the wafer and meanwhile will greatly reduce the local Rayleigh number Ra of the flow in view of the fact that Ra is proportional to the third power of the local wafer-to-chamber top separation distance. Hence it is expected to substantially delay the onset of the buoyancy-driven vortex rolls. But the details on how the vortex flow is affected by the top wall inclination remain poorly understood. To the best knowledge of the present authors, relatively few results were reported in the literature to explore the flow recirculation influenced by the confinement plate inclination. In the present study, we move further to investigate the effects of the top wall inclination on the vortex flow characteristics by conducting experiments for an impinging jet confined in a cylindrical chamber with an inclined top wall. The results will be compared with those without the top wall inclination.

Considerable research has been carried out in the past decades to study the flow and heat transfer in high speed impinging jets in which the jet inertia dominated the flow and the buoyancy exhibited negligible effects. Comprehensive review on the topic up to 1992 was given by Jambunathan et al. [4] and Viskanta [5]. Only the literature directly relevant to the present study is reviewed in the following.

A numerical study of the flow induced in an isothermal confined impinging jet from Deshpande and Vaishnav [6] showed the presence of an inertia force driven circular vortex roll resulting from the jet entrainment and the region occupied by this roll shifted radially outwards with a slight increase in the jet Reynolds number Re_j. But for a further increase in Re_j the vortex roll can move slightly downwards or upwards. Heat transfer characteristics associated with a jet impinging onto a flat surface measured by Huang and El-Genk [7] exhibited the dependence of the Nusselt number not only on the jet Reynolds number, but also on the jet-to-plate separation distance and the radial distance from the stagnation point. Two major differences between the confined and unconfined jets

that affected the local heat transfer rates were considered to be the entrainment of the ambient air and the pressure distribution. Ashforth-Frost and Jambunathan [8] further indicated that the jet potential core was influenced by the length of the confinement, which in turn significantly affected the heat transfer rate at the optimal nozzle-to-plate spacing. Recently, the recirculating flow resulting from a confined jet impinging onto a heated surface has been extensively studied. A rise in the gas flow rate was noted to cause the inner vortex roll driven by the jet inertia to become substantially larger and the outer vortex roll driven by the buoyancy became correspondingly smaller. Besides, the higher buoyancy associated with the larger temperature difference between the plate and jet resulted in a larger outer roll. At higher chamber pressure the Rayleigh number of the flow is higher, resulting in a slightly smaller inner roll and hence a larger outer roll [2,3,9]. It has been noted that the flow of impinging jet can become unstable as the Rayleigh number exceeds certain critical level [3,10–12]. As the Rayleigh number exceeds certain critical level, the buoyancy-driven secondary flow is so strong as to cause the flow transition from a steady state to an unsteady state. Horton and Peterson [13] used the Rayleigh light scattering (RLS) technique to measure the unsteady gas temperature in a simulated vertical CVD chamber and found that the temperature fluctuation increased significantly during the heating cycle due to the buoyancy opposing momentum.

The importance of the buoyancy on the recirculating flow in a vertical CVD reactor was illustrated by Wahl [14]. Similar investigations have been carried out for various types of CVD reactors including the metal organic CVD reactors. In these studies for semiconductor thin film deposition [15–21] various vortex flow patterns were reported in the impinging jet flow. The effects of the chamber top inclination on the thermal and flow characteristics were demonstrated to be rather strong by Kusumoto et al. [15] and Fotiads and Kieda [16]. Buoyancy induced symmetry breaking of the jet flow was noted [12].

In the present study we explore the possible suppression of the buoyancy induced vortex rolls in a confined impinging jet by a gradual downward inclination of the top wall of a vertical cylindrical chamber so that in the wall-jet region the flow is accelerated and meanwhile the local buoyancy is reduced. Experimental flow visualization is conducted to observe the vortex flow in a model processing chamber with an inclined top for various jet flow rates and temperature differences between the wafer and gas jet for two injection nozzles of different diameters. Attention is focused on the vortex flow patterns affected by the inclination of the chamber top. Meanwhile, steady temperature distributions and transient temperature variations will be measured to delineate the steady and unsteady thermal characteristics of the flow.

2. Experimental apparatus and procedures

In order to conduct the experiment at reasonably low cost, we use air as the working fluid to replace the inert gases normally employed in real CVD processes. In view of the similar thermodynamic and thermophysical properties for various gases, the results obtained here are still useful to the design of CVD systems. The two test sections used in the experimental system to investigate the vortex flow characteristics associated with a round air jet impinging vertically downwards onto a circular heated disk confined in a vertical cylindrical chamber with a tapering or a horizontal top are schematically shown in Fig. 1. For clarity, the diagrams in Fig. 1 are not plotted in direct proportion to their actual dimensions. The detailed arrangement of the entire experimental system is already described in our previous study [3] and is not repeated here. The system consists of four major parts—the processing chamber, temperature measurement and data acquisition unit, heating unit, and gas injection unit. The major parts are briefly described in the following.

The processing chamber, which is made of 6.0-mm thick quartz glass to allow for the observation of the vortex flow in it, is cylindrical and has a diameter of 291.0 mm. The vertical distance between the jet inlet and exhaust ports of the processing chamber is 200.0 mm. The chamber can be installed with a horizontal top or an inclined top. For the horizontal top the top-to-disk separation distance is fixed at 20.0 mm (Fig. 1(a)). For the case with the tapering top the top of the processing chamber is inclined linearly downwards in the radial direction. More specifically, the top-to-disk separation distance is reduced from 20.0 mm at the exit of the injection pipe to 10.0 mm at the chamber side (Fig. 1(b)). To facilitate the flow visualization, the two chamber tops are both made of acrylic plates. Air is injected vertically downwards from a long straight circular pipe into the cylindrical chamber along the axis of the chamber and impinges directly onto the heated disk. The air flows first over the heated disk, then moves through the annular section of the chamber, and finally leaves the chamber via twenty circular outlets of 12.7 mm in diameter opened at the bottom of the chamber (Fig. 2(a)). The chamber is sealed to prevent any gas leakage. The top, bottom and side walls of the chamber are thermally well insulated to reduce the heat loss from the processing chamber to the ambient by covering the entire chamber with a superlon insulator of 100.0-mm thick. The insulator can be opened during the flow visualization.

The heating unit is designed to maintain the circular disk at the preset uniform temperature during the

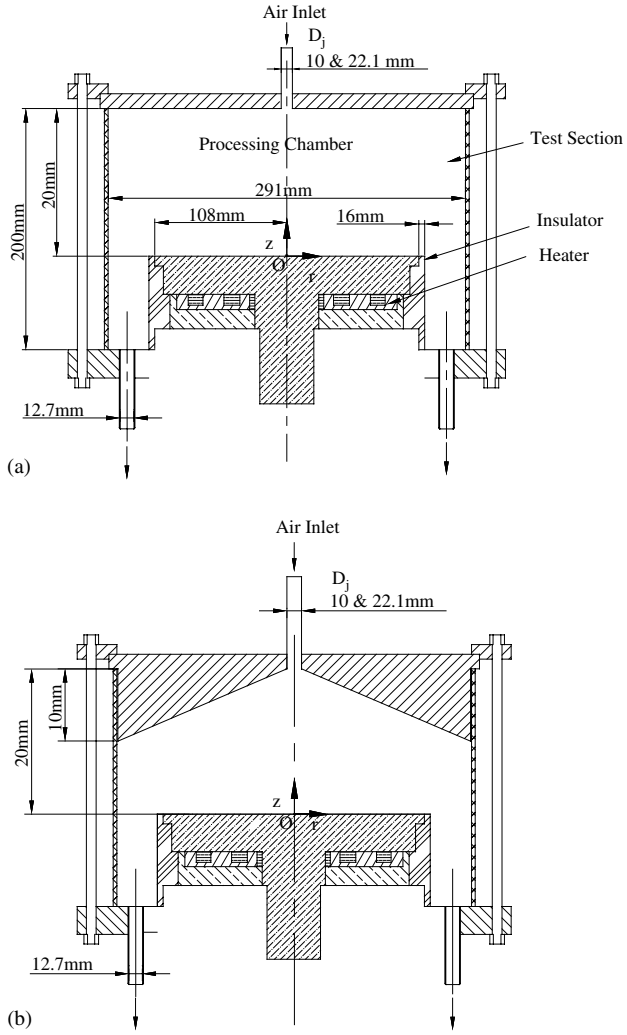

Fig. 1. Schematic diagram of the test section with (a) horizontal and (b) inclined chamber tops. For clear illustration the diagrams are not plotted in proportion to the actual geometrical dimensions.

experiment. It is composed of a 25.0-mm thick high purity circular copper plate of eight-inch in diameter, acting as the disk. The heater attached onto the back side of the copper plate is divided into 3 concentric zones (Fig. 2(b)). Each zone is independently heated by a DC power supply with the DC current passing through the nickel coil placed on a stainless steel base. To reduce the heat loss from the sidewall of the copper plate and stainless steel base, the lateral surface of the entire heating unit is wrapped with a 16.0-mm thick thermal insulation layer of superlon. Care is taken to insure that the outside surface of the insulation layer is smooth and cylindrical. The entire heating unit is then placed on a Teflon plate. A proper control of the voltage from each power supply allows us to maintain the copper plate at a nearly uniform temperature. The measured data indicate that the uncertainty in maintaining the copper plate temperature is ±0.1 °C. No bias in the plate temperature is noted and the plate temperature non-uniformity is spatially random.

The gas injection unit consists of a 2HP air compressor, a flow meter, a smoke generator, filters, pressure regulator, and connection and injection pipes. In the experiments, air is drawn from the ambient by the compressor and sent into a 300-l and 100-psi high-pressure air tank and is filtered to remove moisture and tiny particles. The installation of the high-pressure air tank intends to suppress the fluctuation of the air flow and extends the life of the compressor. Then, the air is mixed with smoke-tracers in the smoke generator and regulated by the pressure regulator, and is later injected into the processing chamber through the straight circular injection pipe which is coaxial with the processing chamber. The downward vertical air jet issuing from the

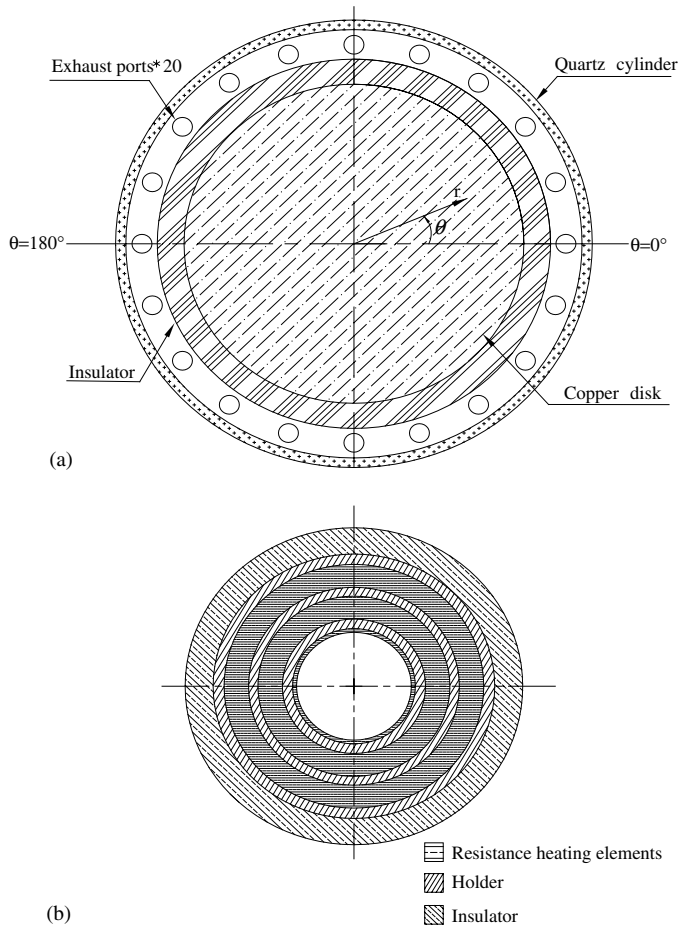

Fig. 2. Schematic of the test section from the top view (a) and 3-zone concentric heater (b).

pipe exit impinges directly onto the heated plate. In the present study, two injection pipes with diameters 10.0 and 22.1 mm are tested and the straight portions of the pipes are both 600.0 mm long. This length of the injection pipes is selected to ensure that they are long enough for the flow to become fully developed in the pipes. The air temperature at 600.0-mm upstream of the exit of the injection pipe is measured by a corrected and calibrated T-type thermocouple. The measured value is considered as the temperature of the air injected into the processing chamber since the whole injection pipe is thermally well insulated by a 16.0-mm layer of superlon insulation.

A smoke-tracer flow visualization technique is employed to observe the flow patterns in the cylindrical chamber. The gas flow pattern is illuminated by the vertical and horizontal plane light sheets produced by passing parallel light sheets from an overhead projector through adjustable knife edges. The experimental system is located in a darkroom to improve the contrast of the flow photos. The time variations of the flow patterns during the entire transient stage from the top and side views are recorded by the Sony digital video camera DCR-PC100. The recorded images are later examined carefully in a personal computer. The air temperature in the processing chamber is measured by inserting a small thermocouple probe into the chamber through small holes of 1.0-mm diameter opened at the top of the chamber. The probe is an OMEGA (model HYPO) mini hypodermic extremely small T-type thermocouple implanted in a 1-in. long stainless steel hypodermic needle.

In the flow visualization experiment the possible distortion of the horizontal light sheet by the curvature of the cylindrical chamber has been inspected by comparing the sizes of the vortex rolls observed from the side and top view flow photos. The results from this comparison indicate that the light distortion associated with the chamber curvature only causes a very slight effect on the images of the vortex flow.

For each case the experiment starts with the air at the room temperature compressed first into the smoke generator through the connection pipe and then injected into the processing chamber. The air moves over the

heated disk and finally leaves the chamber through the outlets at the bottom of the chamber. In the meantime the temperature of the disk and the air flow rate are controlled at the preset levels. As the mixed convective air flow in the processing chamber reaches steady or statistically stable state, we begin to visualize the vortex flow patterns in the chamber.

Uncertainties in the Rayleigh number, jet Reynolds number and other independent parameters are calculated according to the standard procedures established by Kline and McClintock [22]. The uncertainties of the thermophysical properties of the air are also included in the analysis. The properties of the working fluid (air) are $\alpha = 0.22$ (cm^2/s), $\beta = 0.0034$ (K^{-1}), $\nu = 0.16$ (cm^2/s) and $Pr = 0.72$ at 30°C and 1.0 bar. In addition, the uncertainties of the control unsteadiness and temperature non-uniformity are accounted for in the evaluation of the data uncertainty. The analysis shows that the uncertainties of temperature, volume flow rate, dimensions, jet Reynolds number and Rayleigh number measurements are estimated to be less than ±0.2 °C, ±2%, ±0.05 mm, 2.3% and 8.6%, respectively.

To validate our experimental setup, the flow observed in the processing chamber with the horizontal top for the limiting case when the disk is unheated ($Ra = 0$) is compared with the numerical results from Law and Masliyah [23] for the impinging jet flow with a parallel top plate confinement but without the sidewall confinement. It is noted that in the region surrounding the jet axis the resulting vortex flow from our flow visualization is nearly the same as their numerical prediction [3]. Thus, the experimental system established here is considered to be suitable for the present study.

3. Results and discussion

According to the physics of the low speed impinging jet flow with the top plate inclination considered here, several dimensionless governing parameters arise, including the jet Reynolds number Re_j, local Reynolds number in the wall-jet region Re_w, and local and stagnation Rayleigh numbers Ra and Ra_0. They are, respectively, defined as

$$Re_j = \overline{V}_j D_j/\nu = 4Q_j/\pi\nu D_j \tag{1}$$

$$Re_w = \bar{u}r/\nu \tag{2}$$

$$Ra = g\beta\Delta T H^3/\alpha\nu \tag{3}$$

$$Ra_0 = g\beta\Delta T H_0^3/\alpha\nu \tag{4}$$

Here H_0 and H are, respectively, the vertical distances between the disk surface and chamber top at the stagnation point of the impinging jet and at any location on the disk, and $\bar{u}$ is the cross-sectional average of the radial speed of the flow in the wall-jet region. Note that for the chamber with the horizontal top $H = H_0 =$ constant, and $Ra = Ra_0$, but $\bar{u}$ still decreases in the radial direction due to the gradual radial spread of the round impinging jet. Based on global mass balance $\bar{u}$ can be expressed as

$$\bar{u} = Q_j/2\pi rH \tag{5}$$

Hence Re_w can be written as

$$Re_w = Q_j/2\pi\nu H \tag{6}$$

For the chamber with the inclined top, H decreases linearly and Ra reduces cubically with the radial coordinate, as evident from Eq. (3). It should be mentioned that the Grashof number of the flow is defined as $Gr = Ra/Pr$, here Pr is the Prandtl number of air. In the present experiment the jet flow rate Q_j is varied from 1.0 to 5.0 slpm (standard liter per minute) and temperature difference between the heated disk and injected air ΔT is changed form 0 to 35.0 °C for two injection pipes of diameter $D_j = 10.0$ and 22.1 mm with the chamber maintained at the atmospheric pressure. Thus, the jet Reynolds number Re_j ranges from 61 to 676 and the Rayleigh number Ra varies from 0 to 26,300 for the case with the horizontal top. But for the case with the inclined top Ra ranges from 0 to 26,300 at the jet axis and from 0 to 3300 at the chamber side. In what follows selected results from the present flow visualization and temperature measurement are presented to illustrate the effects of the chamber top inclination on the vortex flow associated with the impinging jet in the processing chamber for various jet Reynolds numbers, Rayleigh numbers and injection pipe diameters. The top view flow photos are taken at the horizontal plane 10.0 mm above the heated disk and the side view flow photos are taken at various cross-planes to procure the possible variation of the vortex flow in the circumferential direction at high buoyancy-to-inertia ratios.

3.1. Onset of vortex rolls

The effects of the chamber top inclination on the critical condition for the onset of the inertia- and buoyancy-driven vortex rolls are examined first. Here we detect the onset of the primary and secondary inertia-driven rolls by visualizing the vortex flow in the chamber at increasing jet Reynolds number for an unheated disk ($Ra = 0$). The results for the chamber with the horizontal top have been discussed in our previous study [3]. The side view flow photos were found to be very useful in capturing the very small circular rolls as they just appeared at the onset point. The present results indicate that for the large injection pipe ($D_j = 22.1$ mm) the primary inertia-driven roll is first seen at $Re_j = 18.0$

Table 1
Critical condition for the onset of the buoyancy-driven vortex roll

Jet diameter (D_j, mm)	Chamber top	ΔT (°C)	Q_j (SLPM)	Gr_0	Gr_e	Re_j	Re_{we}	Gr_0/Re_j^2	$(Gr/Re_w^2)_e$
10.0	Horizontal	3.2	6.5	3340	3340	879	55	0.0043	1.1
		4	7	4200	4200	947	59	0.0047	1.2
		5	8	5220	5220	1082	67	0.0045	1.1
	Inclined	5	3	5220	1383	406	40	0.032	0.9
		10	4.2	10,440	2766	568	55	0.036	0.9
22.1	Horizontal	3.2	6.5	3340	3340	398	55	0.021	1.1
		4	7.5	4200	4200	459	59	0.020	1.2
		5	8.5	5220	5220	520	72	0.019	1.0
	Inclined	5	3	5220	1383	184	40	0.154	0.9
		10	4.3	10,440	2766	263	57	0.15	0.9

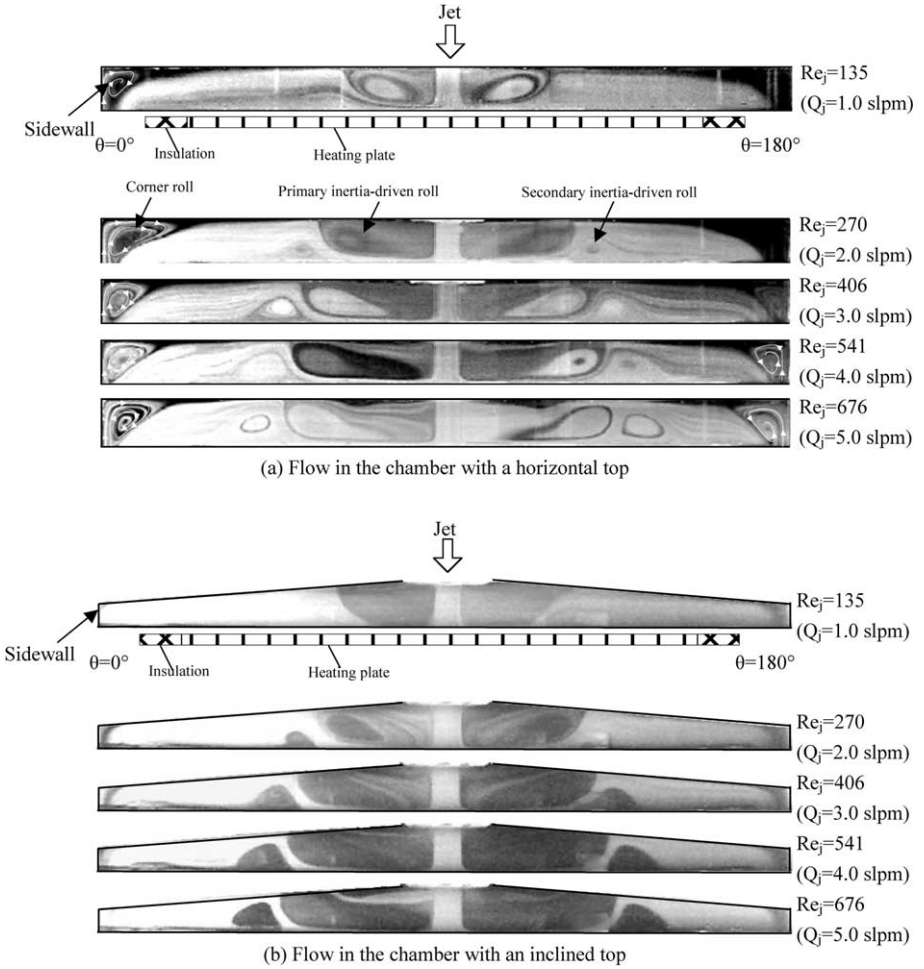

Fig. 3. Steady side view flow photos taken from the chambers with the horizontal top (a) and inclined top (b) at the cross-plane $\theta = 0°$ and 180° for $\Delta T = 0$ °C ($Ra_0 = 0$) and $D_j = 10.0$ mm for various jet flow rates.

when the chamber top is inclined, higher than 15.0 for the chamber with the horizontal top. For the small injection pipe ($D_j = 10.0$ mm) the corresponding onset conditions for the chambers with the inclined and horizontal tops are, respectively, $Re_j = 17$ and 13.6. Further data show that the onset of the secondary inertia-driven roll, respectively, occurs at $Re_j = 240$ and 220 for the inclined and horizontal tops with $D_j = 22.1$ mm. While for $D_j = 10.0$ mm the secondary inertia-driven roll, respectively, emerges at $Re_j = 190$ and 180 for the inclined and horizontal tops. The above results clearly indicate that the chamber top inclination does cause some delay in the onset of both primary and secondary inertia-driven rolls.

It is of interest to note that the present chamber top inclination causes a substantial delay in the onset of the buoyancy-driven roll, as evident from the data summarized in Table 1. More specifically, the average critical buoyancy-to-inertia ratio Gr_0/Re_j^2 is increased drastically from 0.0045 to 0.034 for $D_j = 10.0$ mm and from 0.020 to 0.15 for $D_j = 22.1$ mm when the chamber top is inclined. Thus the chosen chamber top inclination results in a 750% increase in the critical Gr_0/Re_j^2 for the onset of the buoyancy-driven roll.

We further recognize that the initiation of the buoyancy induced roll should depend mainly on the local flow and thermal conditions where it is induced, characterized, respectively, by the local Reynolds number in the wall-jet region Re_w and local Grashof number Gr based on local disk-to-chamber top separation distance. Moreover, the buoyancy induced roll always appears first at the edge of the disk. The data for the local buoyancy-to-inertia ratio Gr/Re_w^2 at the edge of the disk given in Table 1 indeed suggest that the critical $(Gr/Re_w^2)_e$ is all close to 1.0 for different Q_j, ΔT, D_j and chamber top inclination. This can be considered as the universal critical condition for the onset of the buoyancy induced roll in the round impinging gas jet.

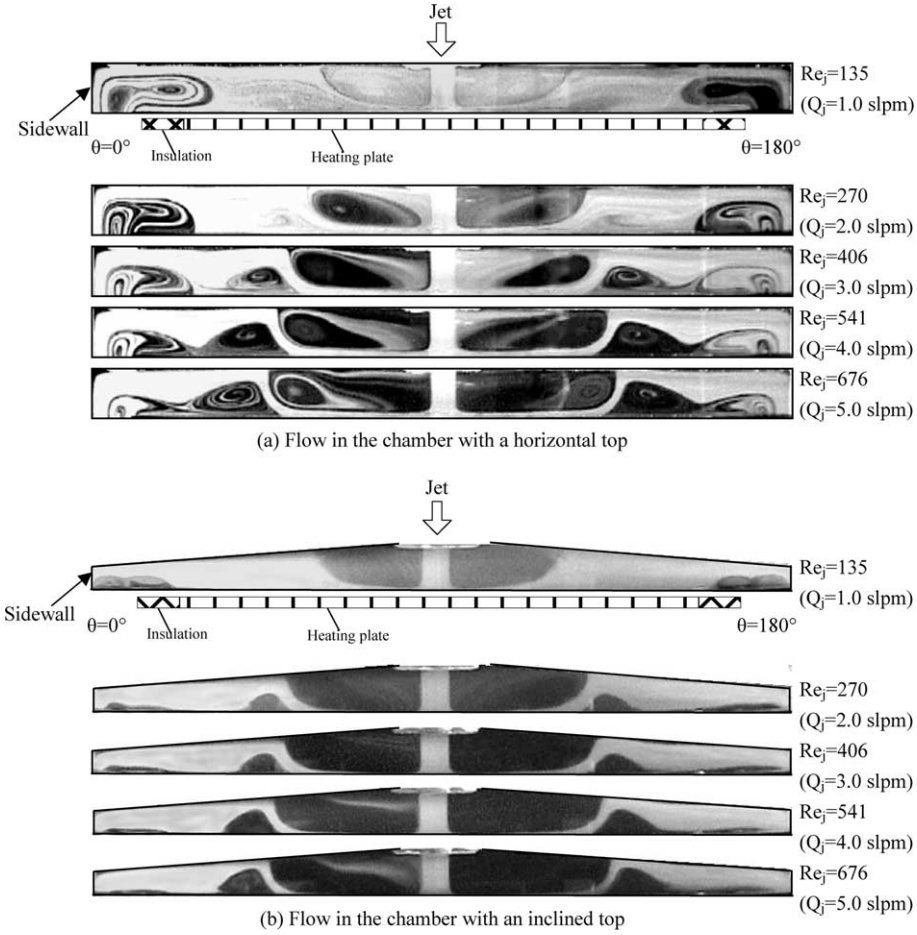

Fig. 4. Steady side view flow photos taken from the chambers with the horizontal top (a) and inclined top (b) at the cross-plane $\theta = 0°$ and 180° for $\Delta T = 5.0$ °C ($Ra_0 = 3760$) and $D_j = 10.0$ mm for various jet flow rates.

3.2. Vortex flow suppression

To illustrate the effects of the chamber top inclination on the recirculating flow in the processing chamber, selected vortex flow patterns at long time in the chambers with the horizontal and inclined tops are compared with each other for the cases with the same Q_j, ΔT and D_j. This comparison is first shown in Fig. 3 for the limiting cases when the disk is unheated ($\Delta T = 0$ °C) for various jet flow rates at $D_j = 10.0$ mm. Since the vortex flow can be more clearly seen from the side view, only the side view flow photos are given here. The results in Fig. 3(a) for the chamber with the horizontal top indicate that in addition to the primary and secondary inertia-driven vortex rolls, we have another circular vortex roll in the corner region of the chamber. This additional roll is not induced by the buoyancy because the disk is unheated and no buoyancy is present in the flow. In fact, this roll emerges from the deflection of the flow from the wall-jet by the chamber side and it is stronger at a higher jet flow rate, which is already discussed in the previous study [3]. It is also noted that the inertia-driven rolls grow significantly in the size and strength at increasing jet flow rate. Now as the chamber top is inclined, no vortex roll appears in the corner region of the chamber for all jet flow rates. The disappearance of the corner roll is conjectured to result from the fact that the flow in the wall-jet region is guided by the inclined top to move obliquely downward along the inclined top and the deflection of the inclined wall-jet flow by the chamber side is much milder. Hence no corner roll is induced. But the inclination of the chamber

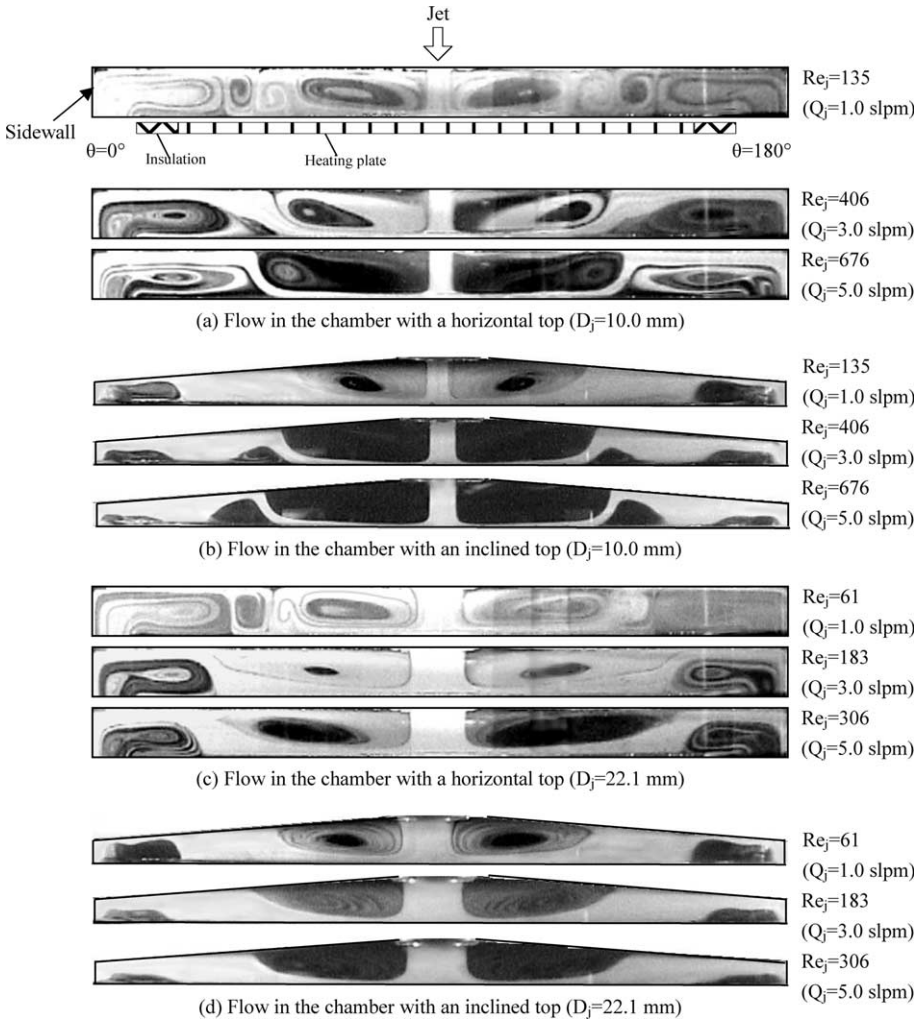

Fig. 5. Side view flow photos at long time taken from the chambers at the cross-plane $\theta = 0°$ and 180° for $\Delta T = 20.0$ °C ($Ra_0 = 15,030$) for various jet flow rates with (a) $D_j = 10.0$ mm and horizontal top, (b) $D_j = 10.0$ mm and inclined top, (c) $D_j = 22.1$ mm and horizontal top and (d) $D_j = 22.1$ mm and inclined top.

top only exerts relatively mild effects on the two inertia-driven rolls. Specifically, for the inclined top the inertia-driven rolls are weaker and smaller to some degree. Similar trend is noted when the jet is injected into the processing chamber through the large injection pipe with $D_j = 22.1$ mm.

Next, the effects of the chamber top inclination on the buoyancy-driven vortex flow are exemplified in Fig. 4 by showing the steady side view flow photos for $\Delta T = 5.0$ °C and $Q_j = 1.0$–5.0 slpm for the chambers with the horizontal and inclined tops for $D_j = 10.0$ mm. The results in Fig. 4(a) for the chamber with the horizontal top indicate that at the low jet flow rate of 1.0 slpm, the buoyancy-driven vortex roll is big and strong. In fact, the buoyancy-induced roll dominates in the outer zone of the chamber. Now as the chamber top is inclined, the buoyancy-driven roll is suppressed significantly and becomes relatively small (Fig. 4(b)). At higher Q_j of 3.0–5.0 slpm the buoyancy-driven roll is completely eliminated by the chamber top inclination. This vortex roll elimination by the chamber top inclination results apparently from the radial flow acceleration and the reduction in the local buoyancy force accompanied with the reducing chamber height in the radial direction. Moreover, it is noted from Fig. 4 that the primary inertia-driven roll is slightly weaker for the inclined chamber top than that for the horizontal chamber top at the same given Ra_0 and Re_j. Even for the much higher ΔT of 20 °C the buoyancy-driven roll is suppressed significantly and the inertia-driven rolls are weakened to some degree by the chamber top inclination, as evident from the results in Fig. 5. Note that at the low Q_j of 1.0 slpm the unstable buoyancy-driven vortex rolls (Fig. 5(a) and (c)) in the chamber with the horizontal top are completely stabilized to become steady and they are significantly suppressed by the chamber top inclination (Fig. 5(b) and (d)). The corresponding top view flow photos indicate that the vortex flow is axisymmetric in the chamber with the inclined top.

We move further to illustrate the effects of the injection pipe diameter on the vortex flow in the chamber with the inclined top. The results indicate that at the same jet flow rate the inertia-driven rolls are somewhat smaller

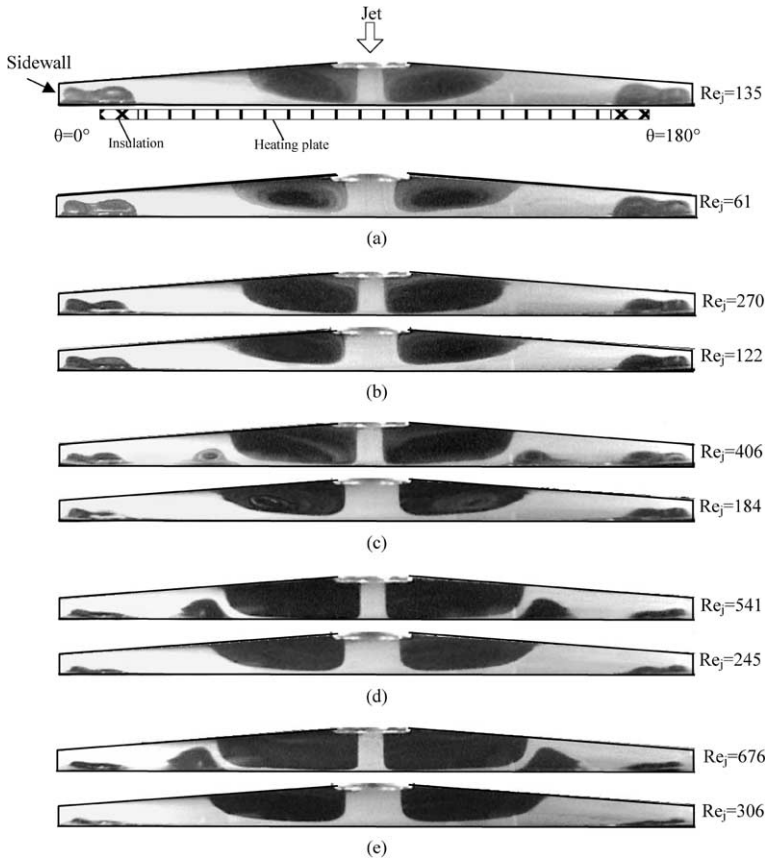

Fig. 6. Steady side view flow photos taken from the chamber with the inclined top at the cross-plane $\theta = 0°$ and 180° for $\Delta T = 15.0$ °C ($Ra_0 = 11,270$), $D_j = 10.0$ and 22.1 mm and $Q_j =$ (a) 1.0 slpm, (b) 2.0 slpm, (c) 3.0 slpm, (d) 4.0 slpm, and (e) 5.0 slpm.

and slightly weaker when the jet is issued from the large injection pipe. However, the buoyancy-driven roll is almost unaffected by the injection pipe diameter, as evident from the results in Fig. 6 for $\Delta T = 15.0$ °C. This is concurrent with the previous observation for the onset of the buoyancy induced vortex flow discussed in Section 3.1 that the buoyancy-driven roll is dominated by the local flow and thermal conditions in wall-jet region in the outer zone of the chamber.

Then, the measured air temperature distributions in the chamber with the inclined top are examined. Fig. 7 shows the steady radial distributions of the dimensionless air temperature defined as $\Phi = (T - T_j)/(T_f - T_j)$ along the horizontal line at $\theta = 0°$ and $z = 5.0$ mm for selected ΔT and Q_j. Note that at given Re_j and Ra_0 the air temperature first increases with the radial distance measured from the jet axis and reaches a maximum at certain r/D_j. For a further increase in the radial distance the air temperature drops gradually. Farther away and near the chamber side at $r > 100.0$ mm the air temperature declines sharply. This large temperature drop in the side wall region results from the fact that some air in the annular section of the chamber, which is at lower temperature than the air near the heated disk, is driven into the space above the heated disk by the buoyancy roll, as evident from the flow photos given in Figs. 4–6. The above non-monotonic radial air temperature distributions result directly from the presence of the counter-rotating primary inertia-driven and buoyancy-driven vortex rolls in the chamber and the deflection of the wall-jet flow by the secondary inertia-driven roll. A close examination of these data further reveals that at increasing jet Reynolds number the temperature peak moves away

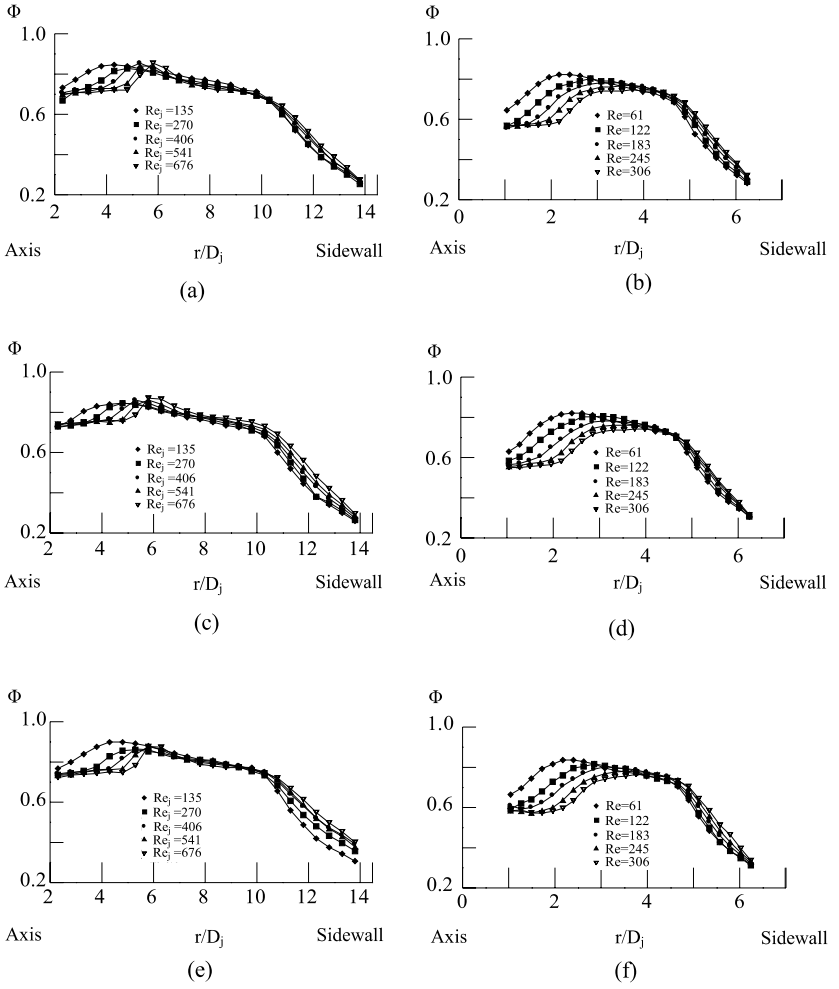

Fig. 7. Steady radial variations of non-dimensional air temperature in the chamber with the inclined top for various Re_j at $z = 5.0$ mm for $Ra_0 =$ (a) 11,270 and $D_j = 10.0$ mm, (b) 11,270 and $D_j = 22.1$ mm, (c) 15,030 and $D_j = 10.0$ mm, (d) 15,030 and $D_j = 22.1$ mm, (e) 18,790 and $D_j = 10.0$ mm, and (f) 18,790 and $D_j = 22.1$ mm.

from the jet axis and the temperature decay in the region near the chamber side is smaller, reflecting from the fact that we have a larger primary inertia-driven roll and a weaker buoyancy-driven roll for a higher Re_j. To further demonstrate the close relationship between the recirculating flow and thermal characteristics in the chamber, we examine the measured steady air temperature distribution and side view flow photo together in Fig. 8 for a typical case with $Re_j = 406$ and $Ra_0 = 15,030$. The horizontal solid line in the photo signifies the locations of temperature measurement. For clear comparison, the corresponding schematical sketch of the vortex flow pattern is also given in Fig. 8. The results in Fig. 8 clearly manifest that in the inner zone of the chamber the air flow near the heated disk in the primary inertia-driven roll gets heated, causing its temperature to increase in the radial direction. But as the wall-jet flow is deflected by the secondary inertia-driven roll to move away from the disk, the air temperature starts to drop. Similar situation is noted for the chamber installed with the large injection pipe.

Finally, the suppression of the temporal flow oscillation driven at high buoyancy-to-inertia ratios by the chamber top inclination is illustrated. Fig. 9(a) and (b), respectively, show the steady and non-periodic cross-plane flows in the chambers with the inclined and horizontal tops for the case with the same Q_j and ΔT ($Q_j = 1.0$ slpm and $\Delta T = 25.0$ °C) for $D_j = 10.0$ mm. Note that at this high buoyancy-to-inertia ratio the

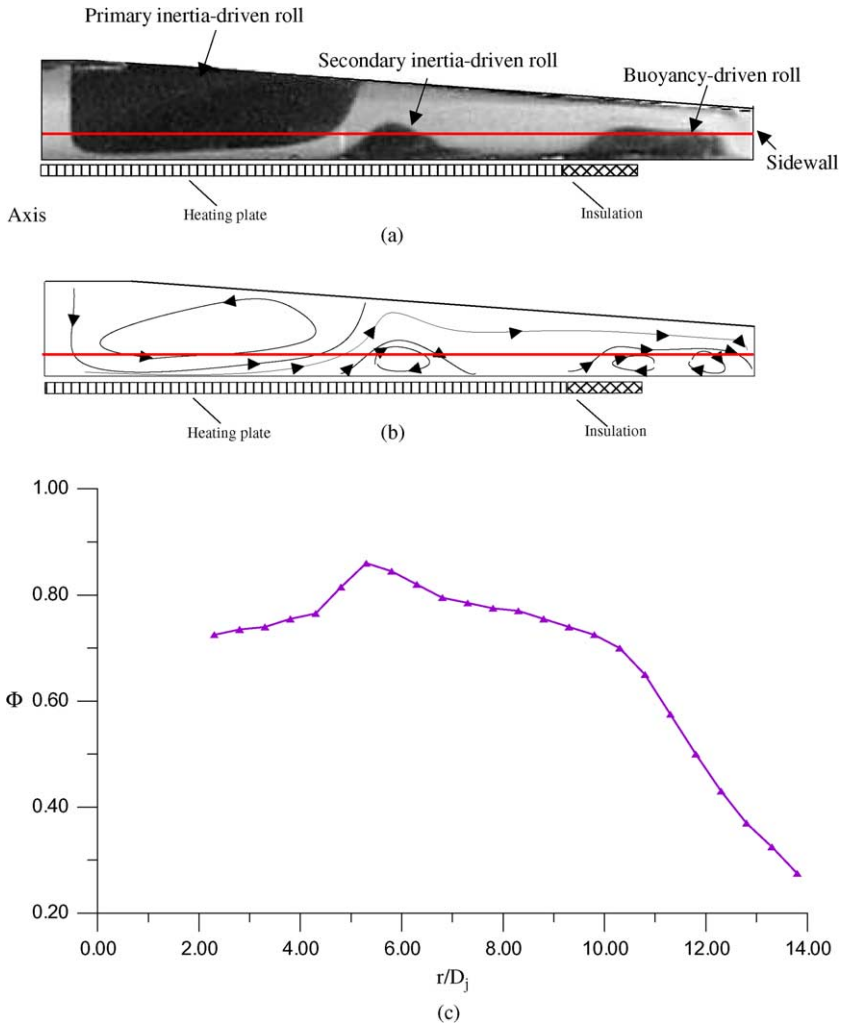

Fig. 8. Steady vortex flow pattern and air temperature distribution at $z = 5.0$ mm in the chamber with the inclined top installed with the small injection pipe ($D_j = 10.0$ mm) at $Re_j = 406$ ($Q_j = 3.0$ slpm) and $Ra_0 = 15,030$ ($\Delta T = 20.0$ °C): (a) steady side view flow photo taken at the cross-plane $\theta = 0°$ and 180°, (b) the corresponding schematically sketched cross-plane vortex flow, and (c) radial variation of non-dimensional steady air temperature.

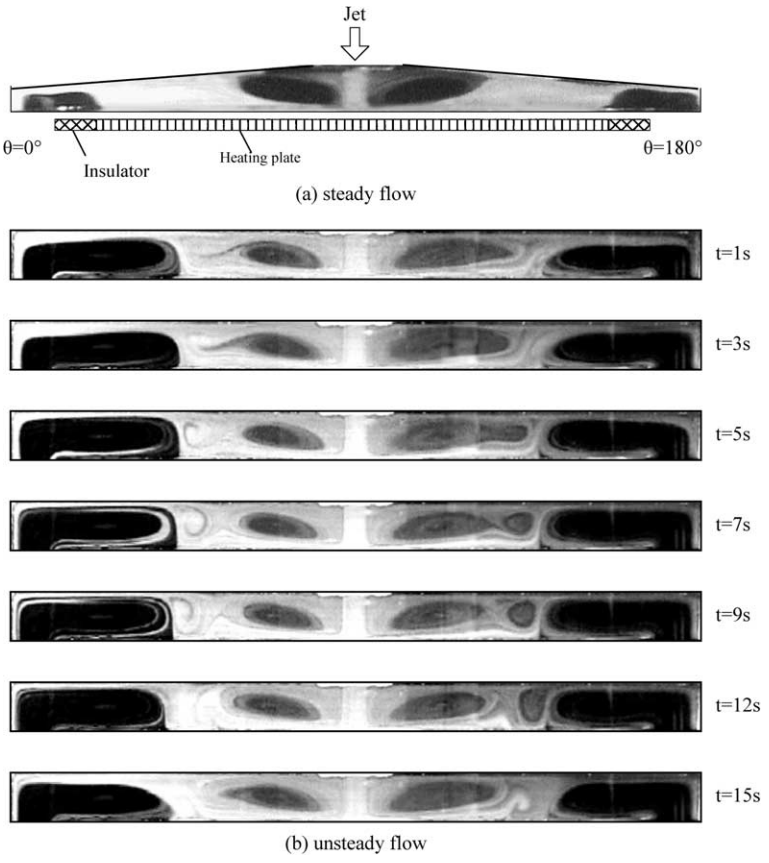

Fig. 9. Steady and unsteady side view flow photos taken at the cross-plane $\theta = 0°$ and 180° for $Q_j = 1.0$ slpm ($Re_j = 61$), $D_j = 10.0$ mm and $\Delta T = 25.0$ °C ($Ra_0 = 18,790$) with (a) the inclined top and (b) the horizontal top.

vortex flow in the chamber with the horizontal top is characterized by the generation, growth, decay and disappearance of the new rolls in a cyclic manner [3]. Thus in the chamber with the horizontal top there is a significant change in the vortex flow pattern with time and the transient temperature data given in Fig. 10(a) suggest that the vortex flow is in a large amplitude time-periodic oscillation. But in the chamber with the inclined top the vortex flow is steady. The above results clearly indicate that the chamber top inclination is very effective in stabilizing the temporal oscillation of the flow. The same trend can be seen for the cases with $Q_j = 1.0$ slpm and an even higher ΔT. Note that at the higher ΔT of 30.0 and 35.0 °C the vortex flow in the chamber with the inclined top is still steady (Fig. 10(b) and (c)).

3.3. Correlations for size and location of vortex rolls

To quantify the effects of the governing parameters on the vortex flow characteristics for the chamber with the inclined top, the data for the maximum radial extent of the inner primary inertia-driven roll S_I, the maximum height of the outer buoyancy-driven roll S_O, and the radial location of the center of the middle secondary inertia-driven roll r_s, are measured from the steady side view flow photos for various cases. The results from this measurement indicate that for the jet issued from the small injection pipe S_I increases almost linearly with the jet Reynolds number Re_j for a given Ra_0, so does the radial location of the middle roll. However, S_O decreases due to an increase in Re_j. We also note that the increase in the size of the inner and outer rolls with the Rayleigh number can be substantial at low Ra_0 especially in the chamber with the jet issued from the large injection pipe. To facilitate the gas flow design in the practical application, empirical equations are proposed to correlate the present data. They can be expressed as

(a) for $D_j = 10$ mm

$$\frac{S_I}{D_j} = 2.138 + 0.00165Re_j + 0.2\left(\frac{Gr_0}{Re_j^2}\right) \tag{7}$$

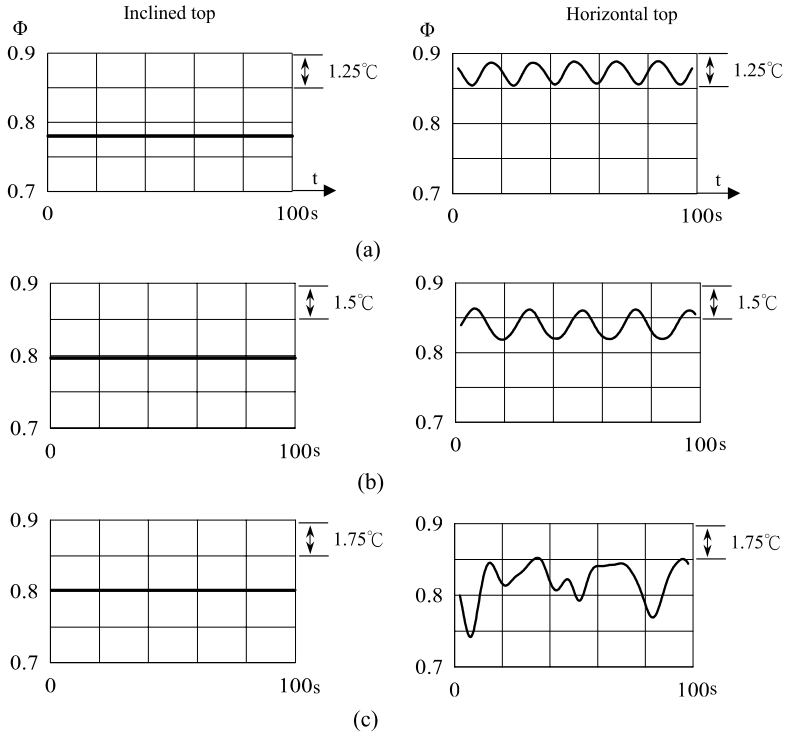

Fig. 10. Time records of non-dimensional air temperature in the chambers with the inclined and horizontal tops for $D_j = 22.1$ mm and $Re_j = 61$ at location $(R, Z) = (0.52, 0.5)$ for horizontal top and (0.52, 0.25) for inclined top for $\theta = 0°$ for various Rayleigh numbers: (a) $Ra_0 = 18,790$ ($\Delta T = 25.0$ °C), (b) $Ra_0 = 22,550$ ($\Delta T = 30.0$ °C) and (c) $Ra_0 = 26,300$ ($\Delta T = 35.0$ °C).

$$\frac{S_O}{H} = 0.485 + 2.6 \times 10^{-4} Re_j + 0.127 \ln\left(\frac{Gr_0}{Re_j^2}\right) \quad (8)$$

$$\frac{r_s}{D_j} = 4.23 - 301.61 Re_j^{-1} + 1.3\left(\frac{Gr_0}{Re_j^2}\right) \quad (9)$$

(b) for $D_j = 22.1$ mm

$$\frac{S_I}{D_j} = 0.733 + 0.002455 Re_j + 0.09648\left(\frac{Gr_0}{Re_j^2}\right) \quad (10)$$

$$\frac{S_O}{H} = -0.03 + 9 \times 10^{-4} Re_j + 0.045 \ln\left(\frac{Gr_0}{Re_j^2}\right) \quad (11)$$

When compared with our experimental data, the standard deviations of Eqs. (7)–(11) are, respectively, 3.3%, 9.8%, 1.5%, 7.3% and 6.7%. The corresponding correlations for the chamber with the horizontal top are available from our previous study [3].

It is recognized that the above correlations are only good for the specific chamber geometry studied here. The results for some other chamber configurations will be reported in the near future.

4. Concluding remarks

An experiment combining flow visualization and transient and steady temperature measurement is conducted in the present study to explore the suppression of the buoyancy-driven vortex flow resulting from a vertically downward air jet impinging onto a heated horizontal circular disk confined in a vertical cylindrical chamber by inclining the top of the chamber. Effects of the inlet gas flow rate, temperature difference between the heated disk and cold air jet, and diameter of the injection pipe on the vortex flow patterns in the chambers with the horizontal and inclined tops have been inspected in detail. The major results obtained in the present study can be briefly summarized in the following:

1. The critical conditions for the appearance of the inertia-driven vortex rolls are delayed to a certain degree by the chamber top inclination. A substantial delay in the onset of the buoyancy-driven roll takes place when the chamber top is inclined. A universal condi-

tion is identified for the onset of the buoyancy-driven vortex roll.
2. The flow acceleration and local buoyancy reduction associated with the chamber top inclination can effectively suppress the buoyancy-driven roll to become smaller and weaker. At low and intermediate buoyancy-to-inertia ratios the buoyancy-driven roll can be completely wiped out. Moreover, at high buoyancy-to-inertia ratios the unsteady vortex flow oscillation can be completely stabilized and the flow becomes steady.
3. The non-monotonic steady air temperature distributions in the radial direction are found to result from the unique vortex flow structure in the chamber.
4. Empirical correlations are provided to quantify the effects of various parameters on the characteristics of the vortex rolls.

It should be mentioned that the experiments conducted here are for the small temperature differences between the jet and heated disk and therefore the variations of the air properties with temperature are small. Hence the present results cannot be directly applicable to the actual CVD system design. Further investigation is needed to investigate the high temperature effects on the flow dynamics in the chamber. During the course of this investigation it is also realized that simple and effective methods to suppress the inertia-driven rolls are also important in practical engineering applications and need to be explored in the future.

Acknowledgements

The financial support of this study by the engineering division of National Science Council of Taiwan, ROC through the contract NSC90-2212-E-009-059 is greatly appreciated.

References

[1] G.B. Stringfellow, Organometallic Vapor Phase Epitaxy: Theory and Practice, Academic Press, San Diego, 1989 (Chapter 5).
[2] T.C. Cheng, P.H. Chiou, T.F. Lin, Visualization of mixed convective vortex rolls in an impinging jet flow of air through a cylindrical chamber, Int. J. Heat Mass Transfer 45 (2002) 3357–3368.
[3] J.C. Hsieh, T.C. Cheng, T.F. Lin, Characteristics of vortex flow in a low speed air jet impinging onto a heated disk in a vertical cylindrical chamber, Int. J. Heat Mass Transfer 46 (2003) 4639–4656.
[4] K. Jambunathan, E. Lai, M.A. Moss, B.L. Button, A review of heat transfer data for single circular jet impingement, Int. J. Heat Fluid Flow 13 (1992) 106–115.
[5] R. Viskanta, Heat transfer to impinging isothermal gas and flame jets, Exp. Therm. Fluid Sci. 6 (1993) 111–134.
[6] M.D. Deshpande, R.N. Vaishnav, Submerged laminar jet impingement on a plane, J. Fluid Mech. 114 (1982) 213–236.
[7] L. Huang, M.S. El-Genk, Heat transfer of an impinging jet on a flat surface, Int. J. Heat Mass Transfer 37 (1994) 1915–1923.
[8] S. Ashforth-Frost, K. Jambunathan, Effect of nozzle geometry and semi-confinement of the potential core of a turbulent axisymmetric, Int. Commun. Heat Mass Transfer 23 (1996) 155–162.
[9] K. Ichimiya, S. Takema, S. Morimoto, T. Kunugi, N. Akino, Movement of impingement heat transfer by a single circular jet with a confined wall, Int. J. Heat Mass Transfer 44 (2001) 3095–3102.
[10] H.V. Santen, C.R. Kleijn, H.E.A.V.D. Akker, Mixed convection in radial flow between horizontal plates—I. Numerical simulations, Trans. ASME, J. Heat Transfer 43 (2000) 1523–1535.
[11] H.V. Santen, C.R. Kleijn, H.E.A.V.D. Akker, Mixed convection in radial flow between horizontal plates—II. Experiments, Trans. ASME, J. Heat Transfer 43 (2000) 1537–1546.
[12] H.V. Santen, C.R. Kleijn, H.E.A.V.D. Akker, Symmetry breaking in a stagnation-flow CVD reactor, J. Cryst. Growth 212 (2000) 311–323.
[13] J.F. Horton, J.E. Peterson, Rayleigh light scattering measurements of transient gas temperature in a rapid chemical vapor deposition reactor, Trans. ASME, J. Heat Transfer 122 (2000) 165–170.
[14] G. Wahl, Hydrodynamic description of CVD processes, Thin Solid Films 40 (1977) 13–26.
[15] Y. Kusumoto, T. Hayashi, S. Komiya, Numerical analysis of the transport phenomena in MOCVD processes, Jpn. J. Appl. Phys. 24 (1985) 620–625.
[16] D.I. Fotiads, S. Kieda, Transport phenomena in vertical reactors for metal organic vapor phase epitaxy, J. Cryst. Growth 102 (1990) 441–470.
[17] A.H. Dilawari, J. Szekely, A mathematical representation of a modified stagnation flow reactor for MOCVD application, J. Cryst. Growth 108 (1991) 491–498.
[18] C.R. Biber, C.A. Wang, S. Motakef, Flow regime map and deposition rate in vertical rotating-disk OMVPE reactor, J. Cryst. Growth 123 (1992) 545–554.
[19] P.N. Gadgil, Optimization of a stagnation point flow reactor design for metal organic chemical vapor deposition by flow visualization, J. Cryst. Growth 134 (1993) 302–312.
[20] C.R. Kleijn, T.H. van der Meer, C.J. Hoogendoorn, A mathematical model for LPCVD in a single wafer reactor, J. Electrochem. Soc. 136 (1989) 3423–3433.
[21] P.N. Gadgil, Single wafer processing in stagnation point flow CVD reactor: prospects, constrains and reactor design, J. Electron. Mater. 22 (1993) 171–177.
[22] S.J. Kline, F.A. McClintock, Describing uncertainties in single-sample experiment, Mech. Eng. 75 (1983) 3–8.
[23] H.S. Law, J.H. Masliyah, Mass transfer due to a confined laminar impinging axisymmetric jet, Int. Eng. Chem. Fundam. 23 (1984) 446–454.